^{197}Au$(n,2n)$ reaction cross section in the 15–21 MeV energy range

A. Kalamara,[1,*] R. Vlastou,[1] M. Kokkoris,[1] N. G. Nicolis,[2] N. Patronis,[2] M. Serris,[3] V. Michalopoulou,[1] A. Stamatopoulos,[1] A. Lagoyannis,[4] and S. Harissopulos[4]

[1]*Department of Physics, National Technical University of Athens, 15780 Athens, Greece*

[2]*Department of Physics, University of Ioannina, 45110 Ioannina, Greece*

[3]*Department of Naval Architecture, Faculty of Technological Applications, Athens University of Applied Sciences, Athens 12210, Greece*

[4]*Institute of Nuclear and Particle Physics, NCSR "Demokritos", 15310 Aghia Paraskevi, Greece*

(Received 13 January 2018; revised manuscript received 8 February 2018; published 22 March 2018)

The cross section of the ^{197}Au$(n,2n)^{196}$Au reaction has been determined at six energies ranging from 15.3–20.9 MeV by means of the activation technique, relative to the ^{27}Al$(n,\alpha)^{24}$Na reaction. Quasimonoenergetic neutron beams were produced via the ^{3}H$(d,n)^{4}$He reaction at the 5.5 MV Tandem T11/25 accelerator laboratory of NCSR "Demokritos". After the irradiations, the induced γ-ray activity of the target and reference foils was measured with high-resolution HPGe detectors. The cross section for the high spin isomeric state (12^-) was determined along with the sum of the ground (2^-), the first (5^+), and second (12^-) isomeric states. Theoretical calculations were carried out with the codes EMPIRE 3.2.2 and TALYS 1.8. Optimum input parameters were chosen in such a way as to simultaneously reproduce several experimental reaction channel cross sections in a satisfactory way, namely the $(n,$elastic$)$, $(n,2n)$, $(n,3n)$, (n,p), (n,α), and $(n,$total$)$ ones.

DOI: 10.1103/PhysRevC.97.034615

I. INTRODUCTION

Neutron-induced reactions on Au are considered as a standard for high-energy neutron dosimetry and are implemented as test cases for many nuclear reaction model codes [1,2]. More specifically, the reaction ^{197}Au$(n,2n)$ leads to the formation of two levels of the residual nucleus ^{196}Au, which present large spin difference (isomeric state, m2: 12^- and ground state g: 2^-). The theoretical study of this reaction, due to the existence of the high spin second metastable, is a powerful tool for obtaining information on the structure of the involved nuclei and thus constitutes an open field of study [3–5]. Above 15 MeV the contribution of preequilibrium emission becomes important and the (n,3n) competing reaction channel opens. Thus, the simultaneous reproduction of the isomeric cross section along with other channels sets a significant constraint, rendering theoretical calculations quite sensitive to the choice of specific nuclear model parameters such as the level density (α) and the spin cutoff (σ^2) ones.

Concerning experimental measurements, although there exist many cross-section data sets in literature [6] for the ground state, this is not the case for the second isomeric state, especially at high neutron beam energies. Above 15 MeV only five data sets exist [7–11] and the corresponding data present significant discrepancies among them. Accurate cross-section values for the population of the high spin isomeric state, which has a much shorter half-life time (m2: $T_{1/2} = 9.6$ h) than the one of the ground state (g: $T_{1/2} = 6.183$ d), could also give an important boost in experimental applications since they offer the possibility for an immediate and less time-consuming activation analysis (when, e.g., Au is used as a reference target for the determination of the neutron fluence).

A few years ago, the same reaction channels have been studied by our group in a different energy region, namely close to the threshold (9.5–10.5 MeV) [4], and the present work constitutes a continuation of the previous one in order to determine the cross section at higher neutron energies, where the existing data are sparse and discrepant. In addition, the theoretical investigation, which was performed at that time using STAPRE-F, EMPIRE 2.19 and TALYS 1.2 codes, could not reproduce well the cross section of the second isomeric state. There was a significant lack of data above 15 MeV, which made the definition of the maximum cross section and its position vague, since many theoretically calculated cross section curves could give acceptable results.

For all the aforementioned reasons, the purpose of this work was to experimentally determine the ^{197}Au$(n,2n)^{196}$Au and ^{197}Au$(n,2n)^{196}$Au^{m2} reaction cross sections at six incident neutron energies ranging from 15.3–20.9 MeV, implementing the activation technique. The measurements were performed at the 5.5 MV Tandem T11/25 accelerator laboratory of NCSR "Demokritos" by means of the ^{3}H$(d,n)^{4}$He reaction, relative to the ^{27}Al$(n,\alpha)^{24}$Na reaction. Additionally, theoretical statistical model calculations were performed over a wide energy range (0.001–35 MeV) and the results were compared to all available experimental data sets in literature. Apart from the measured reactions, ^{197}Au$(n,2n)^{196}$Au and ^{197}Au$(n,2n)^{196}$Au^{m2}, five more reaction channels have been simultaneously reproduced with the same parametrization, using the latest versions of EMPIRE and TALYS codes (3.2.2 [12] and TALYS 1.8 [13], respectively) and the obtained results are quite satisfactory.

*akalamara@central.ntua.gr

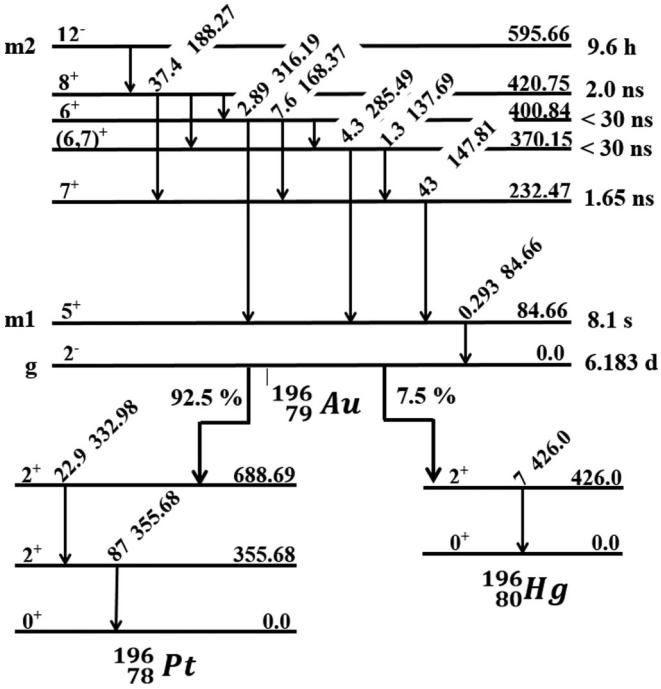

FIG. 1. Simplified decay scheme for the deexcitation of the ground and isomeric states of the ^{196}Au nucleus. The intensities are obtained from the Lund/LBNL library [15] and all energies are given in keV.

II. ^{196}Au NUCLEUS

The residual nucleus of the $(n,2n)$ reaction on ^{197}Au, namely ^{196}Au, is unstable and decays by β^+ emission (92.5%) to ^{196}Pt and by β^- (7.5%) to ^{196}Hg (Fig. 1). The decay half-life of the ground state is 6.183 d and the deexcitation is accompanied by γ-ray emission (with the energies of the three most intense γ rays being 355.7, 333.0, and 426.0 keV). However, the nucleus can be produced in an excited state and populate one of the two isomeric states, which lie at the excitation energies of 84.66 (m1) and 595.66 keV (m2), respectively. The former isomeric state decays with a relatively short half-life of 8.1 s, therefore it is not easy to measure it separately from the ground state, while the latter has a half-life of 9.6 h and thus it can be independently determined (with the energies of the two most intense γ rays from its deexcitation being 147.8 and 188.3 keV).

At this point, it should be noted that the available intensities for the γ rays of the ^{196}Au^{m2} metastable differ remarkably from one library to another (see Table I). In this respect, an effort on determining the correct intensities, guided by Majerle [14], is in progress. Thus, in the present experimental cross-section results, intensity values obtained by the Lund/LBNL library [15] were adopted, as shown in Fig. 1, and cross-section values obtained using the preliminary results of the work mentioned above [14] are also presented.

III. EXPERIMENTAL PROCEDURE

A. Activation

Six irradiations were carried out using neutrons ranging from 15.3–20.9 MeV. The ^{197}Au$(n,2n)^{196}$Au cross-section measurements were performed at the 5.5 MV Tandem T11/25 Accelerator Laboratory of NCSR "Demokritos" implementing the activation method, relative to the ^{27}Al$(n,\alpha)^{24}$Na reaction reference cross section. High purity Au and Al foils of 0.4–0.5 mm in thickness and 13–14 mm in diameter were used for the measurements, while the Au samples were stacked between two Al foils in order to accurately determine the neutron flux.

Quasimonoenergetic neutron beams were produced via the ^{3}H$(d,n)^4$He reaction ($Q = 17.59$ MeV) using a solid Ti-tritiated target described in references [17–19]. The flange with the Ti-T target assembly was air cooled during the irradiations and all the samples were placed at a distance of ∼2 cm from the target flange, thus according to the reaction kinematics the neutrons impinging on the target and reference foils were practically monoenergetic (angular acceptance ±19°).

In order to record the neutron beam fluctuations, a BF_3 detector was placed at a distance of 3 m from the neutron source. The obtained information on the beam instabilities was used in the off-line analysis to correct for the decay of the product nuclei during the irradiation. The main quantities concerning the irradiations are presented in Table II.

TABLE I. γ-ray intensities for the deexcitation of ^{196}Au^{m2} residual nucleus [14–16].

Nucleus	γ-ray energy (keV)	γ-ray intensity (%) TOI [15]	NNDC [16]	Modified values [14]
^{196}Au^{m2}	147.81	43.0	43.5	43.0
	188.27	37.4	30.0	34.0
	168.37	7.6	7.8	5.9
	285.49	4.3	4.4	4.0
	316.19	2.89	3.00	2.80
	137.69	1.3	1.3	1.55

B. γ-ray spectroscopy

Following the end of the irradiations, the induced activity on the Au target and reference foils was measured using three high purity germanium detectors (HPGe) of 100%, 56%, and 16% relative efficiency. All samples were placed at a distance of 10 cm from the detector window, thus there was no need for significant pileup or coincidence summing-effect corrections.

TABLE II. The main quantities concerning the irradiations are presented.

E_d (MeV)	E_n (MeV)	I (μA)	Duration (h)	Neutron fluence (n/cm^2 s)
1.0	15.3 ± 0.5	1.5	26.1	$(3.65 \pm 0.18) \times 10^6$
1.5	17.1 ± 0.3	1.0	96.1	$(2.71 \pm 0.14) \times 10^5$
2.0	17.9 ± 0.3	0.3	9.7	$(2.25 \pm 0.12) \times 10^5$
2.7	18.9 ± 0.3	0.5	27.8	$(3.24 \pm 0.16) \times 10^6$
3.5	20.0 ± 0.2	0.2	10.1	$(1.35 \pm 0.08) \times 10^5$
4.3	20.9 ± 0.2	0.3	32.4	$(2.51 \pm 0.15) \times 10^5$

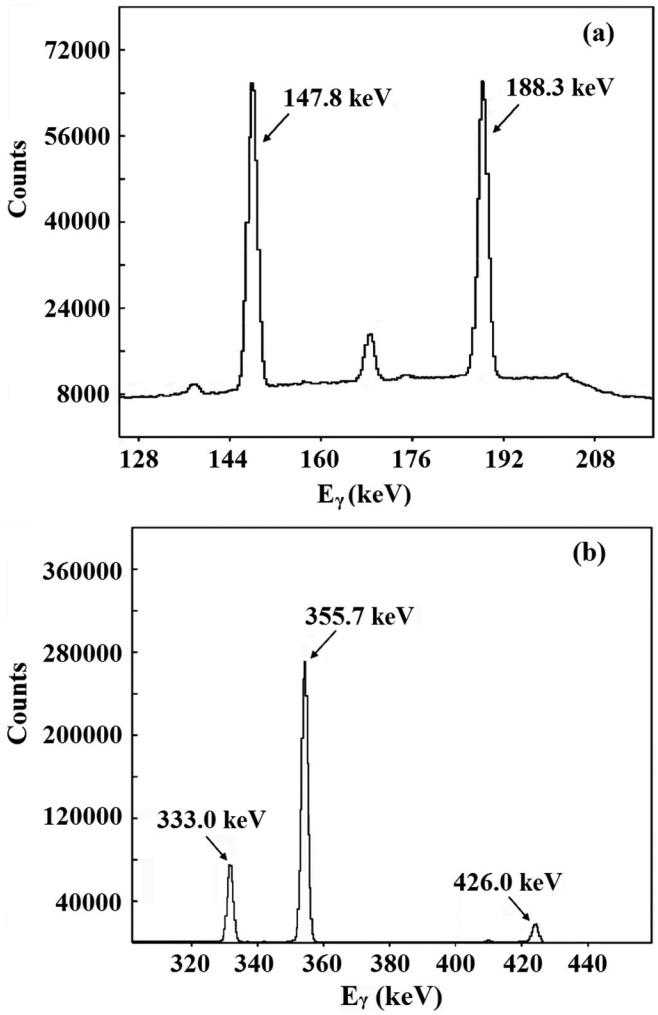

FIG. 2. Off-line γ-ray energy spectra observed after the neutron irradiation at 15.3 MeV. γ-ray transitions from the decay of (a) the second isomeric (m2) and (b) the ground plus both isomeric states (g+m1+m2) are shown. The duration of these measurements was 16 and 19 h, respectively.

At the same distance, a ^{152}Eu point source was implemented in order to determine the absolute efficiency of each detector.

For the population of the second isomeric state (m2), the measurements began ∼1 h after the end of the irradiations and the corresponding cross sections were derived from the two most intense γ rays (147.8 and 188.3 keV) emitted during the deexcitation of the ^{196}Au^{m2} nucleus [11] [see Fig. 2(a)]. In this way, the cross section for this state was independently determined.

Apart from the measurements mentioned above, Au spectra were also taken ∼2 d after the irradiations in order to obtain the cross section of the ground state, when the second metastable state ($T_{1/2}$ = 9.6 h) had fully decayed to the ground one. These cross-section values were obtained as the weighted average using the integral of the 355.7, 333.0, and 426.0 keV γ-ray peaks and as shown in Fig. 1, the population of the ground, first, and second isomeric states was evidently included in the results (g+m1+m2). Typical spectra of gold samples for the (g+m1+m2) cross section are presented in Fig. 2(b), where the γ-ray peaks of interest have been marked. The decay data of the reference and Au targets are presented in Table III.

TABLE III. Decay data for the daughter nuclei [15].

Reaction	$T_{1/2}$	E_γ (keV)	I_γ (%)
^{197}Au(n,2n)^{196}Au$^{g+m1+m2}$	6.183 d	355.7	87.0
		333.0	22.9
		426.0	7.0
^{197}Au(n,2n)^{196}Au^{m2}	9.6 h	147.8	43.0
		188.3	37.4
^{27}Al(n,α)^{24}Na	14.959 h	1368.6	100.0

IV. ANALYSIS

The experimental cross sections were determined using the following expression:

$$\sigma_{\mathrm{Au}} = \sigma_{\mathrm{Al}} \cdot \frac{N_{\gamma_{\mathrm{Au}}}}{N_{\gamma_{\mathrm{Al}}}} \cdot \frac{(\varepsilon_\gamma \cdot I_\gamma \cdot F \cdot D \cdot f_c \cdot N_\tau)_{\mathrm{Al}}}{(\varepsilon_\gamma \cdot I_\gamma \cdot F \cdot D \cdot f_c \cdot N_\tau)_{\mathrm{Au}}} \cdot C_\Phi, \quad (1)$$

where N_γ is the integral of the γ-ray peak in the spectrum obtained with the HPGe detector and ε_γ the absolute efficiency of the detector at the corresponding energy. I_γ is the γ-ray intensity and F is a factor used to correct for γ-ray self-absorption effects in the sample. An additional correction factor, named D, was necessary for the counting collection,

$$D = e^{-\lambda \cdot t_1} - e^{-\lambda \cdot t_2}, \quad (2)$$

where t_1 and t_2 are time intervals from the end of the irradiation to the beginning and termination of the measurement with each HPGe detector, respectively, and λ is the decay constant of the residual nucleus. The fluctuations in the beam flux and the produced nuclei, which decayed during irradiation, were taken into account by means of the f_c factor

$$f_c = \frac{\int_0^{t_B} e^{\lambda t} \cdot f(t) \cdot dt}{\int_0^{t_B} f(t) \cdot dt} \cdot e^{-\lambda \cdot t_B}, \quad (3)$$

where $f(t)$ is the beam flux in arbitrary units as given by the BF_3 counter over specific time intervals and t_B is the irradiation time. The number of the target nuclei, N_τ, was determined via the target mass and the factor C_Φ, which corresponds to the neutron flux ratio in aluminum and gold foils, was estimated within good agreement both experimentally and with Monte Carlo simulations implementing the MCNP5 [20] code.

The cross-section values for the ^{27}Al(n,α)^{24}Na reference reaction were adopted from the IRDFF 1.05 library [21]. Furthermore, in order to estimate the self-absorption correction factor (F), MCNP5 simulations were performed and these corrections were deemed to be essential for the Au samples, since all the γ rays of interest (Table III) have low energies and thus, a high mass attenuation coefficient. In contrast to this effect, the correction for the 1368.6 keV γ ray emitted from the Al reference samples could be considered as being negligible.

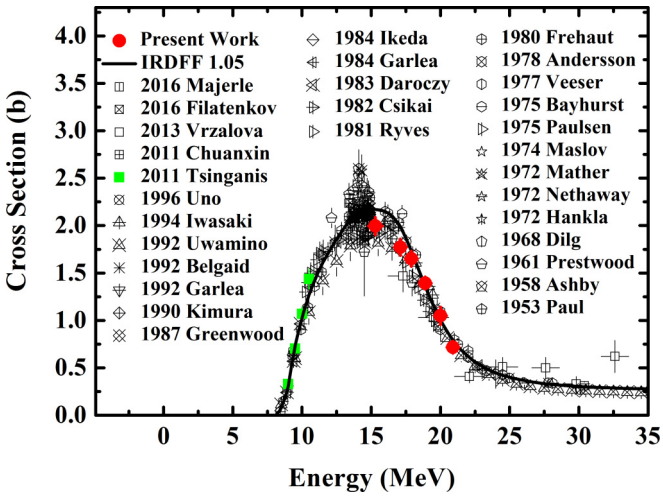

FIG. 3. Experimental cross-section values for the ground and isomeric states of the ^{197}Au$(n,2n)^{196}$Au reaction compared with previous data and IRDFF 1.05 evaluation (solid curve).

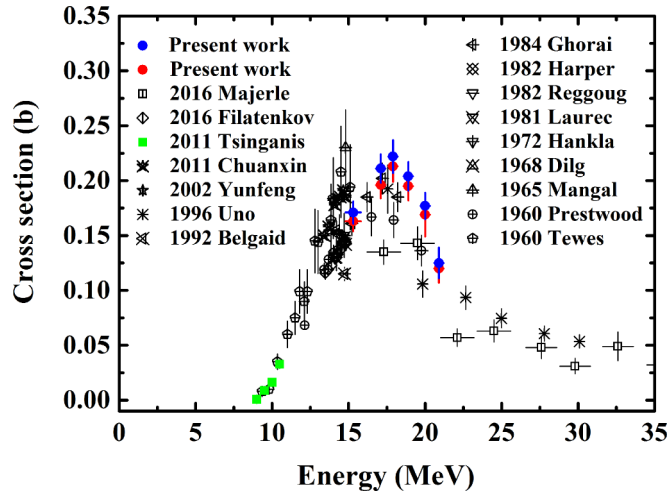

FIG. 4. Experimental cross-section values for the ^{197}Au$(n,2n)^{196}$Au^{m2} reaction. The red points correspond to the values of the third column of Table V, with γ-ray intensities obtained from Ref. [15], while the blue ones are the results presented in the fourth column of Table V, using the modified intensities given in Table I.

V. EXPERIMENTAL CROSS SECTIONS AND UNCERTAINTIES

The experimental cross-section values of this work are presented in Table V along with their corresponding total estimated uncertainties. The results for the sum of the g+m1+m2 cross sections have been deduced using the weighted average of the cross sections obtained via the 355.7, the 333.0, and the 426.0 keV γ lines and are shown in Fig. 3 along with existing experimental data sets in literature and IRDFF 1.05 evaluation results. This evaluation was selected among others due the wide energy range (threshold 60 MeV) of the curve for both studied and reference reactions. Concerning the second isomeric state, the results correspond to the weighted average of the cross sections obtained via the 147.8 and 188.3 keV lines and are presented in Fig. 4. All the experimental results are discussed below, in Sec. VII.

As mentioned explicitly in Ref. [22], a detailed list of all the uncertainty components, their value and a specification of existing correlations is the recommended way to present uncertainties rather than constructing a covariance matrix evaluated by the experimenter. In this respect, the most considerable uncertainties were evaluated and are presented in Table IV. This table consists of five blocks, each corresponding to the uncertainties and results of the cross sections obtained from each γ-ray line at every neutron energy. Since all the factors involved in Eq. (1) were considered uncorrelated, the total uncertainties presented in the third column of Table IV have been deduced by a quadratical summing of all the uncertainties that exist in the same row of the table. However, the correlations between the cross-section measurements for the second isomeric state (m2) obtained from two γ rays were taken into account by determining the weighted average according to Eq. (27) reported in Ref. [47]. In the case of the (g+m1+m2) cross sections, the formalism mentioned in Appendix 2 of Ref. [22] was adopted, since the weighted averages were obtained from three γ rays and three cross-section values, respectively.

VI. THEORETICAL CALCULATIONS

Theoretical cross-section calculations were carried out in the incident neutron energy range between 0.001 and 35 MeV, using the nuclear reaction model codes EMPIRE 3.2.2 [12,23] and TALYS 1.8 [13,24]. In principle in both codes the three basic reaction mechanisms, namely the compound nucleus, preequilibrium emission, and direct reaction ones are taken into account. The final goal of this work was not to compare the two codes with one another (i.e., by using the same input parameters), but rather to determine the optimum combination of nuclear model parameters for each code, which yields the most satisfactory results compared to all the available existing experimental data sets for seven reaction channels, namely for the $(n,\text{elastic})$, $(n,2n)_{g+m1+m2}$, $(n,2n)_{m2}$, $(n,3n)$, (n,p), (n,α), and (n,total) ones. Special attention was devoted to fit the cross section of the isomeric production.

The total angular momentum J of the residual nucleus ^{196}Au is shown in Fig. 5 as a function of excitation energy E. The symbols in this figure show the location of the experimentally known [25] discrete states of ^{196}Au on the (E,J) plane. It has to be noted that there is an absence of known states between the (1.65 ns) 7^- and the second isomeric 12^- state. For comparison, the solid curve shows the rotational energy of the rotating liquid drop model of Ref. [26]. From the statistical model calculations described below, it is known that the partial wave distributions of $n + {}^{196}$Au reactions leading to absorption extend up to about 12 $\hbar$ in the bombarding energy range of the present study. This fact together with the requirement to reproduce the excitation functions of the seven reaction channels imposes stringent constraints in the results of the present calculations.

A. EMPIRE nuclear model code calculations

Compound nucleus reaction cross sections were calculated in the framework of the Hauser-Feshbach theory [27]. The

TABLE IV. The ^{197}Au(n,2n)^{196}Au and ^{197}Au(n,2n)^{196}Au^{m2} cross sections obtained from each γ ray (mentioned in Table III) along with the total uncertainties (in %) and the uncertainties for the most significant contributions in Eq. (1) at each neutron energy.

E_n	Cross section	Uncertainties (%)							
(MeV)	(b)	Total	$(N_\gamma)_{Au}$	$(N_\gamma)_{Al}$	$(N_\tau)_{Au}$	$(N_\tau)_{Al}$	$(\varepsilon_\gamma)_{Au}$	$(\varepsilon_\gamma)_{Al}$	σ_{Al}
For the cross section of the sum of the ground and isomeric states obtained via the analysis of the 355.7 keV γ-ray peak.									
15.3	2.075	4.8	0.1	1.5	0.07	0.45	2.1	2.7	3
17.1	1.913	5.0	1.6	1.5	0.15	0.60	1.6	2.9	3
17.9	1.652	5.3	1.7	1.6	0.07	0.45	2.7	2.7	3
18.9	1.396	5.0	0.2	1.1	0.07	0.55	2.7	2.7	3
20.0	1.024	9.0	2.4	2.1	0.15	0.50	4.8	6.2	3
20.9	0.710	8.7	1.7	0.9	0.15	0.46	4.5	6.2	3
For the cross section of the sum of the ground and isomeric states obtained via the analysis of the 333.0 keV γ-ray peak.									
15.3	2.094	4.8	0.2	1.5	0.07	0.45	2.1	2.7	3
17.1	1.989	4.8	0.6	1.5	0.15	0.60	1.6	2.9	3
17.9	1.723	5.3	1.4	1.6	0.07	0.45	2.6	2.7	3
18.9	1.418	5.0	0.6	1.1	0.07	0.55	2.6	2.7	3
20.0	1.171	10.8	6.3	2.1	0.15	0.50	4.9	6.2	3
20.9	0.724	8.8	1.9	0.9	0.15	0.46	4.6	6.2	3
[a]For the cross section of the sum of the ground and isomeric states obtained via the analysis of the 426.0 keV γ-ray peak.									
15.3	1.896	5.1	1.6	1.5	0.07	0.45	2.2	2.7	3
17.1	1.721	5.0	1.4	1.5	0.15	0.60	1.8	2.9	3
17.9	1.550	6.6	4.2	1.6	0.07	0.45	2.5	2.7	3
18.9	1.372	5.2	1.4	1.1	0.07	0.55	2.5	2.7	3
20.9	0.715	9.8	4.7	0.9	0.15	0.46	4.3	6.2	3
For the cross section of the second isomeric state obtained via the analysis of the 147.8 keV γ-ray peak.									
15.3	0.171	6.5	0.3	1.5	0.07	0.45	4.8	2.7	3
17.1	0.218	6.3	2.3	1.5	0.15	0.60	3.7	2.9	3
17.9	0.218	7.8	2.8	1.6	0.07	0.45	5.9	2.7	3
18.9	0.203	7.4	1.4	1.1	0.07	0.55	5.9	2.7	3
20.0	0.177	14.3	6.2	2.1	0.15	0.50	10.7	6.2	3
20.9	0.124	13.1	2.7	0.9	0.15	0.46	10.7	6.2	3
For the cross section of the second isomeric state obtained via the analysis of the 188.3 keV γ-ray peak.									
15.3	0.156	6.6	0.4	1.5	0.07	0.45	4.9	2.7	3
17.1	0.188	6.7	3.2	1.5	0.15	0.60	3.8	2.9	3
17.9	0.208	8.1	3.0	1.6	0.07	0.45	6.2	2.7	3
18.9	0.188	7.8	2.3	1.1	0.07	0.55	6.2	2.7	3
20.0	0.162	15.0	6.8	2.1	0.15	0.50	11.2	6.2	3
20.9	0.116	13.6	3.2	0.9	0.15	0.46	11.2	6.2	3

[a]For the determination of the cross section of the sum of the ground and isomeric states at 20.0 MeV incident neutron energy, the cross section value obtained from the 426.0 keV γ line was excluded due to the low counting statistics.

default level density formulation of EMPIRE was used, which is based on the enhanced generalized superfluid model (EGSM) [28]. The enhancement compared to the standard GSM corresponds to a more accurate treatment of high angular momenta that affect the spin distribution above the critical excitation energy, where the Fermi gas model is implemented in both the GSM and EGSM [29]. To account for the correlation between the incident and exit channels in elastic scattering, width fluctuation corrections were activated implementing the Hofmann, Richert, Tepel, and Weidenmuller model (HRTW) [30] up to an incident neutron energy of 3 MeV. Concerning the γ-ray emission, γ-ray strength functions were described via modified Lorentzians (MLO1) [31] with parameters available in the RIPL-3 database [25]. The optical model parameters for the outgoing protons were taken from RIPL-3 using the data by Koning *et al.* [32], while parameters obtained by Avrigeanu *et al.* [33] were used for the outgoing α particles.

In order to choose from RIPL-3 the most suitable neutron optical model (OM) potential, extensive tests were carried out and a χ^2 method was used. The existing experimental data [6] for the cross section of the (n,2n) reaction were fitted with a polynomial curve and the latter was used as a guideline to compare with the theoretical predictions. A set of ten calculations of excitation functions was considered with the above setup options and OM parameters for neutrons were taken from Refs. [32,34–40], as presented in Table VI. The

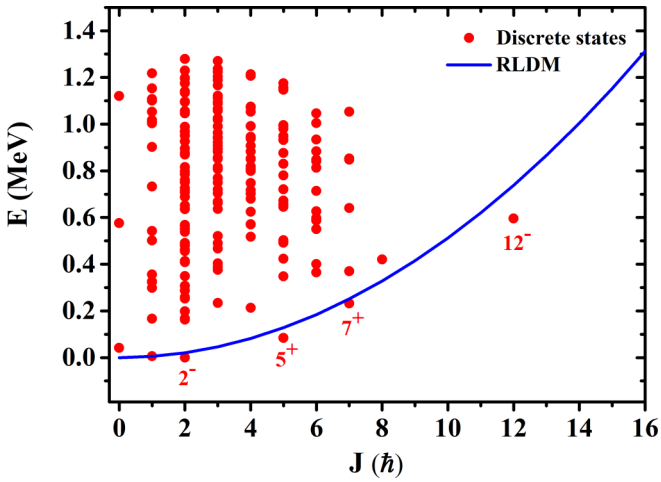

FIG. 5. Location of the experimentally known discrete states of ^{196}Au on the (E,J) plane. The location of the liquid drop model rotational energy [26] is shown with the solid curve.

χ^2 values deduced from the comparison of the theoretical and experimental cross sections are shown in Table VI in the column named $(n,2n)_I$. The best description of the $(n,2n)$ data was obtained with the optical potential options 401 and 430 ([36] and [37], respectively). These calculations reproduced the rest of the reaction channels reasonably well. The χ^2 results improved when the contribution of preequilibrium emission effects was imported in the calculations implementing the classical approach of the exciton model [41] by means of the PCROSS module [12] of the EMPIRE code (PCROSS 2.2). Using this option, the column named $(n,2n)_{II}$ was obtained, as shown in Table VI. The agreement between the calculations and the data improved in all cases except for the OM potentials 2407, 2410, and 2411. The options 401 and 430 provided the best description of the $(n,2n)$ data as well as the rest of the reaction channels. Additionally, special attention was given to the reproduction of the predominant, elastic reaction channel and for this purpose the same χ^2 technique was implemented. The elastic cross-section measurements of neutrons on ^{197}Au in the bombarding energy range 0.3–1.5 MeV [42] have been used to deduce the corresponding guideline. The χ^2 obtained with each of 10 OM potentials is shown in Table VI in the "Elastic" column. The χ^2 values are low for potentials 21, 400, 401, 1464, 1483, and 2405 and high for potentials 430, 2407, 2410, and 2411. On the basis of best agreement with both the $(n,2n)$ and elastic scattering cross sections the OM parameters of Wilmore *et al.* [36] (401) were chosen as the most appropriate.

In the above calculations, the transmission coefficients were calculated by implementing optical model routines via the ECIS06 code [43]. It should be noted that in the calculations the direct reaction channels were suppressed and spherical optical model calculations were performed (DIRECT = 0).

TABLE V. Experimental cross section values and uncertainties for the ^{197}Au$(n,2n)^{196}$Au$^{g+m1+m2}$ and ^{197}Au$(n,2n)^{196}$Au^{m2} reactions. For the cross section of the second metastable two columns are given. In the σ_{m2} column, γ-ray intensity values obtained from Ref. [15] were used, while the σ'_{m2} values were determined using the modified intensities presented in Table I.

E_n (MeV)	$\sigma_{g+m1+m2}$ (mb)	σ_{m2} (mb)	σ'_{m2} (mb)
15.3 ± 0.5	1995 ± 93	163 ± 9	171 ± 10
17.1 ± 0.3	1772 ± 86	196 ± 12	211 ± 13
17.9 ± 0.3	1651 ± 80	213 ± 14	222 ± 15
18.9 ± 0.3	1394 ± 64	195 ± 13	204 ± 13
20.0 ± 0.2	1049 ± 91	169 ± 20	177 ± 12
20.9 ± 0.2	716 ± 56	120 ± 13	125 ± 14

TABLE VI. The optical model potentials that were used in this work and were taken from RIPL-3 [25] are presented. Values of χ^2 are calculated from theoretical and experimental cross sections of the $(n,2n)$ and elastic scattering channels for different optical model potentials. The columns $(n,2n)_I$, $(n,2n)_{II}$, and "Elastic" are explained in the text. The minimum χ^2 values along with the corresponding potential code in RIPL-3 are marked using bold characters.

Code in	Z	A	E (MeV)		χ^2		
RIPL-3	Range	Range	Range	Ref.	$(n,2n)_I$	$(n,2n)_{II}$	Elastic
21	79–79	197–197	0–20	[34]	0.22	0.11	0.01
400	79–79	197–197	0–57	[35]	0.27	0.12	0.01
401	20–92	40–238	0–25	[36]	0.02	**0.01**	**0.01**
430	13–82	27–208	0.1–24	[37]	0.01	0.01	0.16
1464	79–79	197–197	0–200	[32]	0.11	0.03	0.01
1483	79–79	195–200	0–200	[38]	0.15	0.05	0.02
2405	13–83	27–209	0–200	[32]	0.15	0.05	0.01
2407	27–83	59–209	0–200	[39]	0.02	0.10	0.09
2410	13–83	27–209	0–200	[40]	0.02	0.11	0.10
2411	13–83	27–209	0–200	[40]	0.03	0.11	0.09

B. TALYS nuclear model code calculations

TALYS is a nuclear reaction model code that takes into account all the applicable reaction channels depending on the energy region. The compound nucleus reaction cross sections were calculated according to the Hauser-Feshbach theory. Continuous excitation spectra of the nuclei at equilibrium deformation were described with level densities from the generalized superfluid model (GSM). The width of the angular momentum distribution of the level density (spin cutoff parameter, σ^2) is given by the following expression:

$$\sigma^2(E) = 0.01389 \frac{A^{5/3}}{\tilde{\alpha}} \sqrt{\alpha U}, \quad (4)$$

where E is the excitation energy, A is the mass number, α is the level density parameter determined either by experimental information or by global systematics, $\tilde{\alpha}$ is the asymptotic level density parameter one would obtain in the absence of any shell effects [$\tilde{\alpha} = \alpha(E \to \infty)$] and

$$U = E - \Delta, \quad (5)$$

where Δ is an empirical parameter related to the pairing energy, which is included to account for the known odd-even effects in nuclei. In the present work, in order to fairly reproduce the cross section of the second isomeric state the spin cutoff parameter

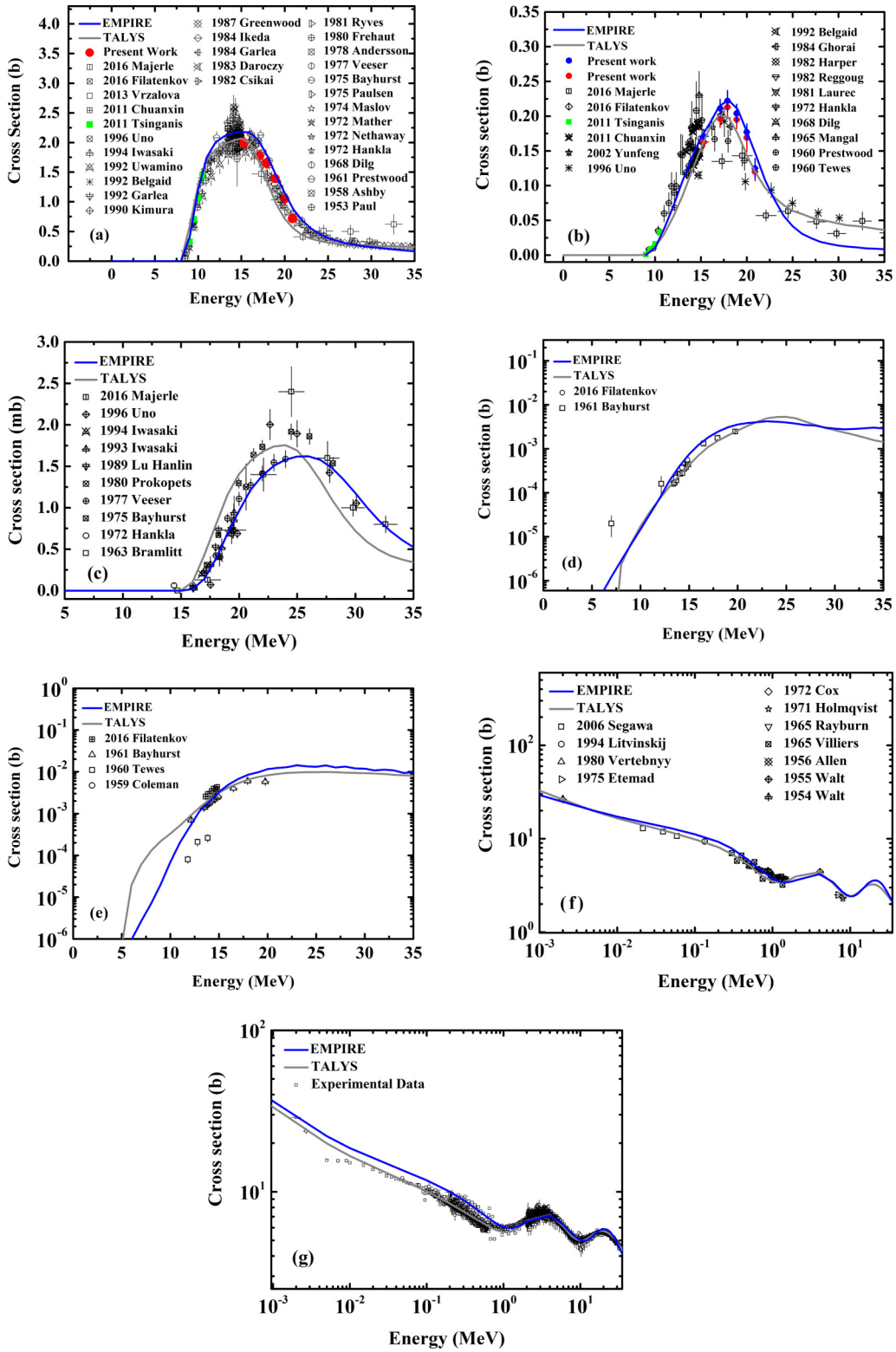

FIG. 6. Cross section of seven reaction channels for the $n + {}^{197}$Au interaction. The experimental results of this work for the (n,2n) channels are presented along with existing data in literature [6] and theoretical calculations obtained with EMPIRE 3.2.2 and TALYS 1.8 codes. Each reaction channel is shown separately: (a) ^{197}Au(n,2n)^{196}Au, (b) ^{197}Au(n,2n)^{196}Au^{m2}, (c) ^{197}Au(n,3n)^{195}Au, (d) ^{197}Au(n,α)^{194}Ir, (e) ^{197}Au(n,p)^{197}Pt^{g+m}, (f) ^{197}Au(n,elastic), and (g) ^{197}Au(n,total).

was multiplied by a factor of 1.5, via the "Rspincut" keyword in TALYS (default value 1). Moreover, the asymptotic level density parameters ($\tilde{\alpha}$) for the ^{198}Au, ^{197}Au, ^{196}Au, and ^{195}Au nuclei were explicitly declared and the values were taken from literature [44] as mentioned in Ref. [4]. Additional width fluctuation corrections were included for neutrons up to 3 MeV using the HRTW model. Regarding γ emission, transitions with a multipolarity up to 4 were taken into account with strength functions calculated microscopically by Goriely according to the Hartree-Fock-Bogolyubov temperature-dependent model. For outgoing neutrons and protons, the global optical model parameters by Koning and Delaroche were used [32], whereas for α particles the parameters by Avrigeanu *et al.* [45] werexbrk adopted.

As far as the preequilibrium deexcitation is concerned, the exciton model was assumed and the transition rates between exciton states were approached numerically with optical model collision probability (preeqmode = 3). Furthermore, the spin distribution for the preequilibrium population of the residual nuclei was chosen to be based on the particle-hole state densities (preeqspin = 3) and an additional adjustment was made for the stripping and pick-up preequilibrium processes for α-particle emission by means of the "Cstrip" keyword, whose value was set to 2 (default 1) [3].

Concerning direct reactions, no spherical OMP calculations were enforced, thus meaning that the coupled-channels method [46] was implemented using a deformed optical model potential. The transmission coefficients were calculated again by means of the ECIS06 code. In any case the direct reaction mechanism contribution to the cross section did not exceed the 8% over the studied energy range, above the $E_{\text{threshold}}$ of the $(n,2n)$ reaction.

VII. RESULTS AND DISCUSSION

The ^{197}Au$(n,2n)^{196}$Au and ^{197}Au$(n,2n)^{196}$Au^{m2} reaction cross sections were measured at six incident neutron energies covering the range between 15.3 and 20.9 MeV and the results are presented in Figs. 3 and 4. The experimental results for the sum of the ground and isomeric states (Fig. 3) follow the general trend indicated by previous data points over the whole energy range. Especially for the cross section on the plateau region ($\sim$14 MeV) the point at 15.3 MeV reveals that the plateau value lies in between the highest and the lowest existing experimental points. Regarding the cross section of the second metastable (Fig. 4), the point at 15.3 MeV agrees with Ghorai *et al.* [8] and Tewes *et al.* [7] within experimental uncertainties. The other ones, ranging from 17.1–20.0 MeV, stand a bit higher than those reported in previous data sets, while the point at 20.9 MeV follows the trend of the points at 19.5, 19.76, and 22.6 MeV by Majerle *et al.* [11], Prestwood *et al.* [10], and Uno *et al.*, respectively. The cross-section values obtained using the modified intensities [14] for the two most intense γ rays (147.8 and 188.3 keV) are slightly higher than the ones determined using the values from the Lund library [15]. However, they agree with one another within their experimental uncertainties and in both cases indicate that the centroid of the cross-section curve is formed at $\sim$17 MeV and not at 15 MeV as one would deduce based on previously existing data points.

The results obtained from EMPIRE 3.2.2 and TALYS 1.8 codes are presented in Fig. 6 along with the data points of this work and already existing experimental datasets from literature [6]. The theoretical calculations from both codes reproduce fairly well all the studied reaction channels. For the cross section of the second metastable [Fig. 6(b)], both codes seem to describe very well the trend of experimental data and agree with the ones obtained in the present work on the position of the cross-section maximum that was mentioned above. In contrast with reference [4], there was no prominent need to reduce the effective moment of inertia. At this point, it should be pointed out that both codes have been considerably improved over the last years. Apart from the fact that this can be easily noticed when comparing the present results with previous ones, i.e., a work from our group by Tsinganis *et al.* [4], it is also explicitly mentioned in Ref. [3] for TALYS 1.8 and in the manual of EMPIRE 3.2 [29] (p. 60). Thus, the high angular momenta treatment in the EGSM in EMPIRE code affects more efficiently the spin distribution above the critical excitation energy, as compared to the GSM, while in TALYS, a small increase of the spin cutoff parameter via the "Rspincut" keyword, was sufficient to successfully reproduce the cross section of the second isomeric state.

Regarding the cross section of the total $(n,2n)$ reaction [Fig. 6(a)], both curves are acceptable, but TALYS probably for incident neutron energies above 15 MeV seems to slightly favor the $(n,3n)$ channel [Fig. 6(c)] over the $(n,2n)$ one. As far as charged particle reaction cross sections are concerned, both codes yield satisfactory results although there is a certain lack of experimental data. Moreover, results for the elastic and total reaction channels also exhibit a very good agreement with existing data over a wide energy range.

VIII. SUMMARY

The ^{197}Au$(n,2n)^{196}$Au and ^{197}Au$(n,2n)^{196}$Au^{m2} reaction cross sections have been measured at six different incident neutron energies ranging from 15.3–20.9 MeV, relative to the ^{27}Al$(n,\alpha)^{24}$Na reaction reference cross section. The new measurements were performed at the 5.5 MV Tandem T11/25 accelerator laboratory of NCSR "Demokritos" in Athens, by means of the activation technique. For the cross section of the ^{197}Au$(n,2n)^{196}$Au reaction, the experimental results are in good agreement with previously existing data and indicate that the maximum value in which the plateau region lies is at $\sim$15 MeV, while for the ^{197}Au$(n,2n)^{196}$Au^{m2} reaction the new data points clearly reveal the whole shape of the cross-section curve with its maximum plateau centered around 17 MeV. Moreover, theoretical cross-section calculations have been performed in the energy range 0.001–35 MeV including the experimental results obtained in the present work along with data from literature for five more competing reaction channels by means of the EMPIRE 3.2.2 and TALYS 1.8 nuclear model codes. Both codes reproduced fairly well all the studied reaction channels, including the isomer production, with a slightly different set of parameters.

ACKNOWLEDGMENTS

Special thanks to M. Majerle for providing us with his preliminary results for the γ-ray intensity values from the

deexcitation of the ^{196}Au^{m2} nucleus and for the fruitful collaboration. In addition, the authors would like to acknowledge the assistance of the accelerator staff at NCSR "Demokritos". This research is implemented through IKY scholarships programme which was financed through the action "Funding scholarship programme for second cycle post-graduate studies" in the framework of the Operational Programme "Human Resources Development Program, Education and Lifelong Learning", 2014-2020 and was co-financed by the European Union (European Social Fund - ESF) and Greek national funds.

[1] I. Sirakov, B. Becker, R. Capote, S. Kopecky, C. Massimi, V. G. Pronyaev, P. Schillebeeckx, A. Trkov, and G. Zerovnik, *Evaluation of Neutron Induced Reaction Cross Sections on Gold* (European Commission, Joint Research Centre, Geel, Belgium, 2013).
[2] L. R. Greenwood and A. L. Nichols, *Review of the Requirements to Improve and Extend the IRDF Library*, International Reactor Dosimetry File (IRDF-2002), IAEA, 2007.
[3] N. Dzysiuk and A. Koning, EPJ Web Conf. **146**, 02047 (2017).
[4] A. Tsinganis, M. Diakaki, M. Kokkoris, A. Lagoyannis, E. Mara, C. T. Papadopoulos, and R. Vlastou, Phys. Rev. C **83**, 024609 (2011).
[5] M. Avrigeanu, V. Avrigeanu, M. Diakaki, and R. Vlastou, Phys. Rev. C **85**, 044618 (2012).
[6] EXFOR, http://www.nndc.bnl.gov/exfor/exfor.htm.
[7] H. A. Tewes, A. A. Caretto, A. E. Miller, and D. R. Nethaway, Lawrence Rad. Lab. (Berkeley and Livermore), No. 6028, p.T (1960) (available in EXFOR).
[8] S. K. Ghorai, K. C. Haworth, J. R. Williams, and W. L. Alford, Bull. Am. Phys. Soc. **29**, 1117 (1984).
[9] Y. Uno, Y. Uwamino, T. S. Soewarsono, and T. Nakamura, Nucl. Sci. Eng. **122**, 247 (1996); Y. Uno, S. Meigo, S. Chiba, T. Fukahori, Y. Kasugai, O. Iwamoto, P. Siegler, and Y. Ikeda, in *Proceedings of the Ninth International Symposium on Reactor Dosimetry, Prague, Czech Republic* (World Scientific, Singapore, 1996), p. 465.
[10] R. J. Prestwood and B. P. Bayhurst, Phys. Rev. **121**, 1438 (1961).
[11] M. Majerle *et al.*, Nucl. Phys. A **953**, 139 (2016).
[12] M. Herman *et al.*, Nucl. Data Sheets **108**, 2655 (2007).
[13] A. Koning, S. Hilaire, and S. Goriely, TALYS-1.8, http://www.talys.eu/fileadmin/talys/user/docs/talys1.8.pdf, 2015.
[14] M. Majerle (private communication).
[15] R. B. Firestone and C. M. Baglin, *Table of Isotopes*, 8th ed. (Wiley, New York, 1999).
[16] NNDC, https://www.nndc.bnl.gov/.
[17] A. Kalamara *et al.*, EPJ Web Conf. **146**, 11048 (2017).
[18] A. Kalamara, R. Vlastou, M. Kokkoris, M. Diakaki, A. Tsinganis, N. Patronis, M. Axiotis, and A. Lagoyannis, Phys. Rev. C **93**, 014610 (2016).
[19] R. Vlastou *et al.*, Physics Procedia **66**, 425 (2015).
[20] X-5 Monte Carlo team, MCNP-A General Monte Carlo N-ParticleTransport Code, version 5, Volume I-III, LA-UR-03-1987, LA-CP-03 0245 and LA-CP-03-0284, April 2003.
[21] ENDF, https://www-nds.iaea.org/exfor/endf.htm.
[22] W. Mannhart, A Small Guide to Generating Covariances of Experimental Data, IAEA, INDC(NDS)-0588 Rev., 2013.
[23] https://www-nds.iaea.org/index-meeting-crp/EmpireWorkshop2013/downloadEmpire322win.htm.
[24] http://www.talys.eu/download-talys/.
[25] R. Capote *et al.*, https://www-nds.iaea.org/RIPL-3/, 2009.
[26] S. Cohen, F. Plasil, and W. J. Swiatecki, Ann. Phys. (NY) **82**, 557 (1974).
[27] W. Hauser and H. Feshbach, Phys. Rev. **87**, 366 (1952).
[28] A. D'Arrigo *et al.*, J. Phys. G **20**, 365 (1994).
[29] https://www-nds.iaea.org/index-meeting-crp/EmpireWorkshop2013/docs/empire-3.2.pdf.
[30] H. M. Hofmann *et al.*, Ann. Phys. (NY) **90**, 403 (1975).
[31] V. A. Plujko, Acta Phys. Pol. B **31**, 435 (2000).
[32] A. J. Koning and J. P. Delaroche, Nucl. Phys. A **713**, 231 (2003).
[33] V. Avrigeanu, P. E. Hodgson, and M. Avrigeanu, Phys. Rev. C **49**, 2136 (1994).
[34] R. C. Harper and W. L. Alford, J. Phys. G: Nucl. Phys. **8**, 153 (1982).
[35] J. P. Delaroche, International Conference on Neutron Physics for Reactors, Harwell, 1978.
[36] D. Wilmore and P. E. Hodgson, Nucl. Phys. **55**, 673 (1964).
[37] O. Bersillon and N. Cindro, Fifth International Symposium on Interactions of Fast Neutrons with Nuclei, Gaussig, 1975.
[38] R. Capote, M. Herman, P. Obložinsky, P. G. Young, S. Goriely, T. Belgya, A. V. Ignatyuk, A. J. Koning, S. Hilaire, V. A. Plujko, M. Avrigeanu, O. Bersillon, M. B. Chadwick, T. Fukahori, Zhigang Ge, Yinlu Han, S. Kailas, J. Kopecky, V. M. Maslov, G. Reffo, M. Sin, E. Sh. Soukhovitskii, and P. Talou, Nucl. Data Sheets **110**, 3107 (2009) (RIPL paper).
[39] B. Morillon and P. Romain, Phys. Rev. C **70**, 014601 (2004); **74**, 014601 (2006).
[40] B. Morillon and P. Romain, Phys. Rev. C **76**, 044601 (2007).
[41] J. J. Griffin, Phys. Rev. Lett. **17**, 478 (1966).
[42] J. A. M. De Villiers *et al.*, Z. Phys. **183**, 323 (1965).
[43] J. Raynal, *Optical-Model and Coupled-Channel Calculations in Nuclear Physics*, International Atomic Energy Agency Report IAEA-SMR-9/8 (IAEA, Vienna, 1972), pp. 281–322, ICTP International Seminar Course: Computing as a language of physics, Trieste, Italy, 1971.
[44] T. Belgya *et al.*, IAEA-TECDOC-1506, https://www-nds.iaea.org/RIPL-2/, 2006.
[45] V. Avrigeanu, M. Avrigeanu, and C. Mănăilescu, Phys. Rev. C **90**, 044612 (2014).
[46] T. Tamura, Rev. Mod. Phys. **37**, 679 (1965).
[47] N. Otuka *et al.*, Radiat. Phys. Chem. **140**, 502 (2017).